DESIGN OF PROPELLERS FOR MOTORSOARERS

E. Eugene Larrabee
Massachusetts Institute of Technology

SUMMARY

An efficient method has been developed for the design of propellers of minimum induced loss matched to an arbitrary operating point characterized by disc loading (thrust or power), air density, shaft speed, flight speed, and number of blades. A consistent procedure is outlined to predict the performance of these propellers under off-design conditions, or to predict the performance of propellers of general geometry. These procedures are particularly helpful for motorsoarer constructors and propeller builders constrained to use unusual powerplants under unusual conditions. The examples discussed include a man powered airplane, a hang glider with a 7.5 kW (10 hp) 8,000 rpm engine, and an airplane-like motorsoarer.

INTRODUCTION

For wings and propellers alike, there are spanwise or radial circulation distributions which minimize the kinetic energy loss associated with the generation of lift or thrust. These circulation distributions give rise to simple induced velocity distributions which help determine efficient wing or blade geometry. Everyone is familiar with the elliptic span loading and the corresponding uniform downwash velocity of the vortex sheet shed by a wing of minimum induced drag, but not so many are familiar with the Betz-Prandtl (ref. 1) or Goldstein (ref. 2) radial circulation functions and the corresponding uniform "displacement velocity" of the helicoidal vortex sheets shed by a propeller of minimum induced loss. The purpose of this paper is to demonstrate the application of these ideas to geometry determination and performance prediction for propellers of motorsoarers and other unusual aircraft. I have discussed some of these ideas in another paper (ref. 3). See Table I for notation used in this paper.

THE DISPLACEMENT VELOCITY

Consider an elementary helical vortex filament lying in an helicoidal vortex sheet which forms part of the slipstream of a propeller, as shown in figure 1. The vortex filament is constrained to move everywhere perpendicular to itself with a velocity w_s, which is the same as the local slipstream velocity. If the filament helix angle is ϕ_s, the axial velocity of the filament is $w_s \cos \phi_s$ and its angular velocity is $w_s \sin \phi_s / r_s$, where r_s is the helix radius. If we were unaware of the helix angular velocity, however, we would

suppose that it had only a underlined displacement velocity $v' = w_s/\cos\phi_s$, in the same way that a rotating barber pole has a displacement velocity even though it has no axial velocity.

Betz, in reference 1, was the first to show that the condition for minimum induced loss operation of a propeller (or a windmill, for that matter) corresponds to radially constant displacement velocity. The axial and swirl components of the vortex sheet motion are then given by

$$w_{axial} = v' \cos^2 \phi_s \tag{1}$$

$$w_{swirl} = v' \cos \phi_s \sin \phi_s \tag{2}$$

MOTION OF THE ENTIRE SLIPSTREAM

Prandtl, in an appendix to reference 1, pointed out that the slipstream fluid between the vortex sheets moves at a fraction F of the sheet velocity, which he evaluated by analogy with the known solution for the flow about an infinite array of semi-infinite plates moving perpendicular to themselves with velocity v, as shown in figure 2. The plate solution spacing parameter, f, is recalculated according to the helicoidal vortex sheet spacing and the radial distance from the outer edges of the sheets:

$$f = \frac{B}{2} \frac{\sqrt{\lambda^2 + 1}}{\lambda} (1 - \frac{r}{R}) \tag{3}$$

Here λ is the advance ratio

$$\lambda \equiv V/\Omega R = (V/nD)/\pi \tag{4}$$

and B is the number of blades; slipstream distortion is neglected. The corresponding underlined average axial and swirl velocities at a certain radius in the slipstream are then

$$\overline{w}_{axial} = F v' \cos^2 \phi_s \tag{1a}$$

$$\overline{w}_{swirl} = F v' \cos \phi_s \sin \phi_s \tag{2a}$$

$$F = (2/\pi) \cos^{-1} (e^{-f}) \tag{5}$$

286

THE RADIAL CIRCULATION DISTRIBUTION

The radial circulation function corresponding to this minimum induced loss slipstream motion is found by setting the circulation about a slipstream tube equal to the total vorticity trailed by the blades at the corresponding radius, and introducing "light loading" approximations:

$$B\Gamma = 2\pi \; r_s \; F \; v' \; \cos \phi_s \; \sin \phi_s \tag{6}$$

$$r_s \cong r \tag{7}$$

$$\phi_s \cong \phi \tag{8}$$

$$\phi \cong \tan^{-1}(V/\Omega r) \tag{9}$$

The resulting circulation function is conveniently.written in a normalized form

$$\frac{B\Omega\Gamma}{2\pi V v'} = \frac{F \; x^2}{x^2 + 1} \equiv G \tag{10}$$

(G for Goldstein or Glauert) where

$$x \equiv \Omega r/V = (r/R)/\lambda \tag{11}$$

Equation 10 seems too simple to be true. Goldstein, in his doctor's thesis (ref. 2), verified its essential correctness, however, for propellers operating at low advance ratios or with many blades, where the vortex sheets are nearly flat, parallel, and closely spaced. The Prandtl-Betz and Goldstein circulation functions are compared in figure 3. It should be noted that a radial plot of G is identical with a radial plot of the ratio of the average axial slipstream velocity (increment) to the displacement velocity.

DETERMINATION OF THE DISPLACEMENT VELOCITY

Following Goldstein (ref. 2) we relate the displacement velocity to the disc loading (thrust or torque) by resolving Joukowsky's law into two orthogonal components:

$$\left(\frac{dT}{dr}\right)_L = \rho \Omega r \; (1 - a') \; \Gamma B \tag{12a}$$

$$\left(\frac{1}{r} \frac{dQ}{dr}\right)_L = \rho V \; (1 + a) \; \Gamma B \tag{12b}$$

Here the subscript "L" means that only the lift forces are being considered,

and a' and a are the swirl and axial components of the induced velocity at the lifting lines. Retaining the light loading assumptions, and taking the induced velocities to be half the vortex <u>sheet</u> velocities in the developed slipstream, we obtain:

$$a' = \frac{1}{2} \frac{v'}{\Omega r} \cos \phi_s \sin \phi_s \cong \frac{1}{2} \left(\frac{v'}{V}\right) \frac{1}{x^2 + 1} \tag{13a}$$

$$a = \frac{1}{2} \frac{v'}{V} \cos^2 \phi_s \cong \frac{1}{2} \left(\frac{v'}{V}\right) \frac{x^2}{x^2 + 1} \tag{13b}$$

The circulation is given by the Betz-Prandtl approximation:

$$\Gamma = \left(\frac{2\pi V v'}{B\Omega}\right) G \tag{10 restated}$$

The blade profile drag contributions to thrust and torque are given by

$$\left(\frac{dT}{dr}\right)_D = - \left(\frac{D}{L}\right) \frac{dL}{dr} \sin \phi \cong - \frac{D}{L} \left(\frac{dT}{dr}\right)_L \frac{1}{x} \tag{14a}$$

$$\left(\frac{1}{r} \frac{dQ}{dr}\right)_D = + \left(\frac{D}{L}\right) \frac{dL}{dr} \cos \phi \cong + \frac{D}{L} \left(\frac{1}{r} \frac{dQ}{dr}\right)_L x \tag{14b}$$

The radial gradients of thrust coefficient, $T_c \equiv 2T/\rho V^2 \pi R^2$, and power coefficient, $P_c \equiv 2P/\rho V^3 \pi R^2$, finally may be written as

$$\frac{dT_c}{d\xi} = \frac{dI_1}{d\xi} \zeta - \frac{dI_2}{d\xi} \zeta^2 \tag{15a}$$

$$\frac{dP_c}{d\xi} = \frac{dJ_1}{d\xi} + \frac{dJ_2}{d\xi} \zeta^2 \tag{15b}$$

where $\xi \equiv r/R$, $\zeta = v'/V$, and

$$\frac{dI_1}{d\xi} = 4 \xi G \left(1 - \frac{D/L}{x}\right) \tag{16}$$

$$\frac{dI_2}{d\xi} = 2 \xi G \left(1 - \frac{D/L}{x}\right) \left(\frac{1}{x^2 + 1}\right) \tag{17}$$

$$\frac{dJ_1}{d\xi} = 4 \xi G \left(1 + \frac{D}{L} x\right) \tag{18}$$

$$\frac{dJ_2}{d\xi} = 2 \xi G \left(1 + \frac{D}{L} x\right) \left(\frac{x^2}{x^2 + 1}\right) \tag{19}$$

Equations 16, 17, 18, and 19 can be numerically integrated radially to give four integrals I_1, I_2, J_1, and J_2 which depend only on λ and B and the presumed radial distribution of profile D/L ratio. The displacement velocity ratio is then easily found with these integrals and the propeller disc loading:

$$\zeta = \frac{I_1}{2I_2} \left[1 - \sqrt{1 - \frac{4T_c I_2}{I_1^2}} \right] \quad \text{(thrust)} \tag{20a}$$

$$\zeta = \frac{J_1}{2J_2} \left[\sqrt{1 + \frac{4P_c J_2}{J_1^2}} - 1 \right] \quad \text{(power)} \tag{20b}$$

Equations 20a and 20b are the propeller counterpart of the induced angle of attack of an elliptically loaded wing, $C_L/\pi(b^2/S)$.

If the propeller is to absorb a given amount of power, one calculates the power coefficient, P_c, and the displacement velocity ratio, ζ, from equation 20b; the thrust coefficient and the efficiency are then given by $T_c = I_1\zeta - I_2\zeta^2$ and $\eta = T_c/P_c$, respectively. The alternate procedure, when the thrust is specified, is obvious.

For moderately loaded propellers operating at low advance ratios, equations 20a or 20b may give values of ζ which are large compared to λ. In this case a second approximation of the radial gradients of thrust and power coefficient is given by

$$\frac{dT_c}{d\xi} = 4 \zeta \lambda G \left(\frac{W}{V}\right) \left[\cos \phi - \frac{D}{L} \sin \phi\right] \tag{21}$$

$$\frac{dP_c}{d\xi} = 4 \zeta \xi G \left(\frac{W}{V}\right) \left[\sin \phi + \frac{D}{L} \cos \phi\right] \tag{22}$$

where

$$\phi = \tan^{-1} \left[\frac{\lambda}{\xi}\left(1 + \frac{\zeta}{2}\right)\right] \tag{23}$$

and

$$\frac{W}{V} = \sqrt{x^2 + 1 - \left[\frac{1}{2} \zeta \cos \phi\right]^2} \tag{24}$$

Equations 21 and 22 can then be integrated radially to find better values of T_c and P_c appropriate to the value of ζ obtained from equation 20a or 20b. Following Theodorsen (ref. 4), one might consider a third level approximation in which $G(\lambda,B)$ is recalculated with a "vortex advance ratio", $\lambda_v = \lambda(1+\zeta/2)$, to account for slipstream distortion.

DETERMINATION OF THE PROPELLER GEOMETRY

The propeller chord distribution is controlled by the choice of lift coefficient for the required circulation:

$$\frac{1}{2} \rho \, W^2 \, c \, c_\ell = \rho \, W \, \Gamma = \rho \, W \, \frac{2\pi V v'}{B\Omega} \quad (G) \tag{25}$$

This can be written as $\frac{c}{R} = \frac{4\pi\lambda}{B} \frac{G}{(W/V)} \frac{\zeta}{c_\ell} \simeq \frac{4\pi\lambda}{B} \frac{G}{\sqrt{x^2+1}} \frac{\zeta}{c_\ell}$ (26)

Lift coefficients must be chosen with regard to structural constraints on thickness-to-chord ratios at inner radii and local Mach numbers at outer radii; also they must be consistent with the D/L ratios that have been used to find ζ. Some consideration must be given to off-design conditions as well; for example, a propeller designed for cruise can be expected to develop larger lift coefficient increases at inner radii than at outer radii when it is operated at lower advance ratios, as in climbing flight.

Traditionally propellers have been built with flat bottom airfoil sections such as the Clark Y. Considering the large thickness-to-chord ratios needed structurally at the inner radii, and the inherent variation of lift coefficient with camber (proportional to thickness-to-chord ratio), one can design the propeller to operate with radially constant zero angle of attack. In this case the propeller will have constant "true geometric pitch", given by:

$$\frac{P_{geometric}}{Diameter} = \pi\lambda\left(1 + \frac{1}{2}\zeta\right), \quad \alpha = 0 \tag{27}$$

Modern computational airfoil theory (ref. 5) shows that the lift coefficient for Clark Y airfoils of varying thickness-to-chord ratio is given by

$$c_\ell = 0.062 + 4.21(t/c) + 0.0971 \, \alpha°; \quad 0.07 < \frac{t}{c} < 0.19$$

when they are operated at a Reynolds number of 1×10^6 and a Mach number of 0.2.

The theory presented so far has assumed uniform flow at flight velocity V through the propeller disc at vanishingly small values of ζ. This is not a realistic assumption for propellers turned by direct drive piston engines which are often quite large compared to the propeller radius. If the axial velocity distribution, averaged around the propeller disc at radius r, is given by $\bar{u}V$, it is customary to "depitch the propeller" ($\bar{u}(\xi)<1$) so that the blade angle is given by

$$\beta = \tan^{-1}\left[\frac{\bar{u}\lambda}{\xi}\left(1 + \frac{\zeta}{2}\right)\right] + \alpha \tag{28}$$

This has the effect of preserving the prescribed circulation function. The performance consequences of propeller-fuselage interaction are considered in the next section.

290

PERFORMANCE OF ARBITRARY PROPELLERS

Unlike an untwisted elliptical planform wing, which has elliptic loading over a range of angles of attack, a minimum-induced loss propeller has minimum induced loss loading only at its design advance ratio. An arbitrary propeller theory is needed to calculate its off-design point performance, or the performance of any general propeller. The theory given here is a radially graded momentum theory like Glauert's (refs. 6 and 7), but it will return the design performance of a minimum induced loss propeller when applied to the design conditions and geometry calculated by the methods described before.

The axial and swirl components of the induced velocity at the blade elements are found by setting the changes of axial and swirl momentum within a given annulus of the slipstream equal to the axial and torque loading of the corresponding blade elements as shown in figure 4:

$$\frac{dT}{dr} = 2\pi r \rho V \ (\overline{u} + a) \ 2FaV$$

$$= \frac{\rho}{2} V^2 \left[\frac{\overline{u} + a}{\sin \phi}\right]^2 \left(\frac{Bc}{2\pi r}\right) 2\pi r \ C_y \tag{29}$$

$$\frac{1}{r} \frac{dQ}{dr} = 2\pi r \rho V \ (\overline{u} + a) \ 2F\Omega r a'$$

$$= \frac{\rho}{2} V^2 \left[\frac{\overline{u} + a}{\sin \phi}\right]^2 \left(\frac{Bc}{2\pi r}\right) 2\pi r \ C_x \tag{30}$$

where (see figure 4)

$$\phi = \tan^{-1}\left[\frac{V}{\Omega r} \frac{(\overline{u} + a)}{(1 - a')}\right] \tag{31}$$

$$C_y = c_\ell \cos \phi - c_d \sin \phi \tag{32}$$

$$C_x = c_\ell \sin \phi + c_d \cos \phi \tag{33}$$

In the absence of the propeller, the velocity in the flow field about the fuselage or nacelle is assumed to be given by an average axial component u and an average radial component v at a distance r from the propeller shaft. We account for only the axial component

$$\overline{u} = u/V \tag{34}$$

Equations 29 and 30 can be solved for the induced velocity components in terms of the dimensionless thrust and torque loading:

$$\frac{a}{\overline{u} + a} = \frac{1}{4} \frac{\sigma C_y}{\sin^2\phi} \frac{1}{F} \ ; \ \sigma \equiv \frac{Bc}{2\pi r} \tag{35}$$

$$\frac{a'}{1 - a'} = \frac{1}{4} \frac{\sigma C_x}{\sin\phi \ \cos\phi} \frac{1}{F} \tag{36}$$

Equations similiar to these appear in Glauert's article in Durand's "Aerodyna-mic Theory" (ref. 7), with the vortex spacing factor F in the numerator in-stead of the denominator, just as his widow and R. McKinnon Wood left them.

The induced velocity components are evaluated at each radial station by an iterative process outlined below:

At each value of ξ the following are known:

ξ, λ, F, σ, β, $\overline{u}$; $c_\ell = c_\ell(\alpha)$, $c_d = c_d(c_\ell)$

Choose α_1

Calculate $\phi_{\alpha_1} = \beta - \alpha_1$

Calculate c_ℓ, c_d

Calculate C_y, C_x (eqs. 32 and 33)

Calculate a and a' (eqs. 35 and 36)

Calculate $\phi_{a_1} = \tan^{-1}\left[\dfrac{\lambda}{\xi}\dfrac{(\overline{u} + a)}{(1 - a')}\right]$

Calculate $\phi_{\alpha_1} - \phi_{a_1}$

if $\phi_{\alpha_1} - \phi_{a_1} > 0$, $\alpha_2 < \alpha_1$

if $\phi_{\alpha_1} - \phi_{a_1} < 0$, $\alpha_2 > \alpha_1$

Iterate until $\left|\phi_{\alpha_n} - \phi_{a_n}\right|$ is less than some small quantity.

Retain ϕ_n, C_{y_n}, C_{x_n}, a_n, a'_n

The wing theory analog of this computation is to suppose that the induced angle of attack at any spanwise station y of a non-elliptically loaded wing of span b is given by

$$\alpha_{induced} = \frac{1}{4}\frac{(c/b)c_\ell}{\sqrt{1 - (2y/b)^2}} \tag{37}$$

where c and c_ℓ are the chord and section lift coefficient at the same station. The quantity $\sqrt{1 - (2y/b)^2}$ vanishes at y = b/2 in the same way that F vanishes at r = R, and it may be shown that equation 37 yields $\alpha_{induced} = C_L/\pi(b^2/S)$ for an elliptically loaded wing of elliptic planform.

The values of ϕ, C_y, C_x, and a' are then integrated radially to find the thrust load and the power absorption of the propeller in the fuselage (or nacelle) flow field. These may be conveniently written in terms of coeffi-cients based on the shaft speed n (revolutions/sec)

$$C_T = \frac{T}{\rho n^2 D^4} \quad (D = 2R) \tag{38}$$

292

$$C_P = \frac{P}{\rho n^3 D^5} \tag{39}$$

$$\frac{dC_T}{d\xi} = \frac{\pi^3}{4} \left(\frac{1 - a'}{\cos \phi}\right)^2 \xi^3 \sigma C_y \tag{40}$$

$$\frac{dC_P}{d\xi} = \frac{\pi^4}{4} \left(\frac{1 - a'}{\cos \phi}\right)^2 \xi^4 \sigma C_x \tag{41}$$

The a', cos ϕ choice is preferred for numerical precision over the a, sin ϕ, u choice.

The thrusting propeller is surrounded by a static pressure field with an appreciable axial variation, both upstream and downstream. Koning (ref. 8) has estimated its value:

$$\frac{\Delta P}{\frac{\rho}{2} V^2} = + \frac{T_c}{2} \left(1 - \frac{x/R}{\sqrt{(x/R)^2 + 1}}\right) \quad \begin{array}{l}\text{downstream;}\\ \text{tractor propeller}\end{array} \tag{42}$$

$$\frac{\Delta P}{\frac{\rho}{2} V^2} = - \frac{T_c}{2} \left(1 + \frac{x/R}{\sqrt{(x/R)^2 + 1}}\right) \quad \begin{array}{l}\text{upstream;}\\ \text{pusher propeller}\end{array} \tag{43}$$

Here x is distance downstream from the propeller. This axial pressure gradient causes the propeller-bearing-fuselage or nacelle to have a buoyancy drag given by

$$\Delta C_{D_{buoyancy}} = \frac{1}{S_{ref}} \int_0^\ell \left(\frac{\Delta P}{\frac{\rho}{2} V^2}\right) \left(\frac{dS_b}{dx_b}\right) dx_b \tag{44}$$

where S_{ref} is the reference area for drag coefficients, ℓ is the body length, and S_b is the body cross section area at the distance x_b behind the body nose. The net thrust of the propeller-body combination is then given by,

$$C_{T_n} = C_T \left(1 - \frac{S_{ref} \Delta C_{D_{buoyancy}}}{\pi R^2}\right) \tag{45}$$

while the installed efficiency of the propeller becomes

$$\eta = \frac{C_{T_n} (\pi \lambda)}{C_P} = \frac{C_{T_n} (V/nD)}{C_P} \tag{46}$$

Figure 5 shows an application of the arbitrary propeller theory just described to the prediction of the performance of a scale model of a light airplane propeller when tested as an "isolated" propeller, and when run at the nose of a representative fuselage. This theory is computationally more demanding than the design theory presented in the previous section since it requires extensive estimates of the propeller airfoil section properties at several radii, a good estimate of the three dimensional flow field surrounding the

fuselage (or nacelle) at the propeller location, an iteration procedure to determine the induced velocities, and numerical integrations to determine blade loading and body buoyancy drag in the propeller pressure field. Limited experience with it at M.I.T. shows that it gives reasonable results, and these are being experimentally confirmed (1979). In common with other radially graded momentum theories it fails to take account of the effect of circulation at every radial station on the downwash (or "inflow") at a particular station, but it is made to be consistent with the induced velocity pattern for a minimum induced loss propeller through Prandtl's analytic vortex spacing velocity fraction F rather than through tabulated values of Goldstein's circulation function. The next step up to a "prescribed" or "free" discrete vortex model of the "rotor" and its "wake" is much more diffcult.

APPLICATIONS

(1) Man powered airplane. Here we redesign the "Gossamer Condor" propeller. The design conditions, summarized in figure 6, correspond to climbing flight in ground effect at an angle of 1°; approximately 30% of the 53.3 N (11.8 lbs) of thrust is required to overcome the component of airplane weight along the flight path. The figure shows the radial variation of profile D/L ratio and the radial gradients of the integrals I_1, I_2, J_1, and J_2. The design thrust coefficient, $T_c = 0.3175$, requires a displacement velocity ratio, $\zeta = 0.2671$, which corresponds to a power coefficient, $P_c = 0.3914$, and an efficiency, $\eta = 0.8113$. The powerplant output required is 328 watts (0.44 hp).

Since the displacement velocity ratio is moderately large, it is worthwhile to recalculate the thrust coefficient and the power coefficient using eqs. 21-24. The results are summarized in figure 7, which also compares the propeller geometry determined by the methods of this paper with the geometry actually employed. The agreement of blade angles is very good, especially when one takes into account the difference between the zero lift angles of the Clark Y airfoils assumed in the design calculations and the Stratford pressure recovery airfoils used on the "Gossamer Condor". In my opinion the propeller calculated here would be more efficient than the one actually flown.

(2) Powered hang glider. Soarmaster, Inc. supplies a powerpack consisting of a West Bend (Chrysler) two stroke, single cylinder engine developing 7.46 kW (10 hp) at 10,000 rpm, a centrifugal clutch, a chain and sprocket reduction gear, and an extension shaft turning a pusher propeller. This is a suitable powerplant for hang gliders of 12 m (40 ft) span; figure 8 presents the options available for propellers intended to absorb the engine power at a flight speed of 13 m/sec (30 mph). The diameter of the direct drive propeller is limited to 690 mm (27 in) by a tip Mach number of 0.85; its efficiency is very poor because of the excessive disc loading. Gear reductions and larger propellers lead to progressive improvements in performance. Figure 9 gives the geometry of the largest propeller considered, a 1372 mm (54 in) diameter propeller turned at 1946 rpm by a 9:37 sprocket pair driven at 8000 rpm. It has 617 mm (24 in) nominal pitch, and the typical wide root chord – narrow tip chord geometry of a propeller matched to a low advance ratio; this is in spite of a

design lift coefficient of 1 near the hub and 0.5 at the tip. Soarmaster supplies two propeller options: a 1067 x 483 mm (42 x 19 in) or an 1118 x 356 mm (44 x 14 in) "laminar" airscrew, both of fiber reinforced plastic.

Table 2 summarizes the propeller parameters covered in this study: when two values are given for T_c, P_c, and η, the second set corresponds to the improved velocity polygon geometry corresponding to eqs. 21-24; note the relatively good agreement, even for ζ values of more than 1. Examination of figure 9 and Table 2 suggests that still larger propellers and larger reduction ratios would improve climbing performance; this has to be balanced against the weight penalty and the reduction of ground clearance at the tail.

(3) Motorsoarer. The Ryson ST-100 is a 17.58 m (57.67 ft) span two seated aircraft, with a flying mass of 748.4 kg (1650 lbs), fitted with a Hoffmann HO-V-62 propeller of 1.7 m (67 in) diameter. This propeller has a low pitch setting, a high pitch setting, and can be feathered for glider mode operation. Figure 10 shows three design points which might be considered in the selection of such a propeller: sea level climbing performance at 40 m/sec (90 mph); sea level top speed at about 68 m/sec (152 mph); and cruise at 75% power at full throttle at 1981 m (6500 ft) altitude and 65 m/sec (145 mph). The circled points show the performance that may reasonably be expected from minimum induced loss propellers designed for each of these flight conditions by the methods of the paper.

Figure 11 shows how a compromise propeller may be designed which will give nearly this performance at two of these points. The displacement velocities are calculated assuming minimum induced loss loading and a somewhat pessimistic radial distribution of D/L ratio. Blade lift coefficients are assigned at $\xi = 0.3$ and $\xi = 0.7$ so that the blade chord to radius ratio, c/R, as given by equation 26, is the same for both flight conditions. The c/R ratio is then calculated at other radii, assuming a linear radial variation of c_ℓ. Reasonable assumptions are then made about the radial variation of thickness to chord ratio, t/c, to give the radial variation of blade angle (eq. 28). The compromise c/R ratio and blade twist, $\Delta\beta$, are then chosen to minimize differences between the two conditions. In general, highly loaded, low advance ratio flight conditions demand high lift coefficients near the hub Betz (ref. 9) was of the opinion that Coriolis forces within the rotating blade boundary layer favored such a distribution.

REFERENCES

1. Betz, Albert (with an appendix by Ludwig Prandtl): Schraubenpropeller mit geringstem Energieverlust (Screw propellers with Minimum Energy Loss). Goettingen Reports, 1919.

2. Goldstein, Sidney: On the Vortex Theory of Screw Propellers. Proceedings of the Royal Society, 1929 (his doctor's thesis).

3. Larrabee, E. Eugune: Practical Design of Minimum Induced Loss Propellers. SAE preprint for the April 1979 Business Aircraft Meeting and Exposition, Wichita, Kansas.

4. Theodorsen, Theodore: Theory of Propellers. McGraw-Hill Book Company, Inc. 1948.

5. Smetana, Frederick O., et al.: Light Aircraft Lift, Drag, and Moment Prediction – A Review and Analysis. NASA Contractor's Report CR-2523.

6. Glauert, H.: Elements of Aerofoil and Airscrew Theory. Cambridge, 1926.

7. Glauert, H.: Airplane Propellers. Div. L, Vol IV of Durand's "Aerodynamic Theory" Springer Verlag 1935; also Dover reprint.

8. Koning, C.: Influence of the Propeller on Other Parts of the Airplane Structure. Division M, Vol IV ibid.

9. Betz, Albert: Hoechsauftrieb von Fluegeln an umlaufenden Raedern (Maximum Lift of Blades on Running Rotors). Flugwissenschaft 9 (1961) Heft 4/5 Seiten 97-99.

TABLE I

SYMBOLS AND NOTATION (follows Glauert; ref. 8)

aV	axial component of induced velocity (m/sec)
$a'\Omega r$	rotational (swirl) component of induced velocity (m/sec)
B	number of blades
b	wing span (m)
c	blade chord (m)
c_d	section (profile) drag coefficient
c_ℓ	section (profile) lift coefficient
C_L	wing lift coefficient
C_p	power coefficient ($C_p \equiv P/\rho n^3 D^5$)
C_T	thrust coefficient ($C_T \equiv T/\rho n^2 D^4$)
C_x	blade element torque load coefficient
C_y	blade element thrust load coefficient
D	drag; also propeller diameter (m)
F	slipstream velocity fraction (eq. 5)
f	vortex sheet spacing parameter (eq. 3)
G	circulation radial distribution function (eqs. 10,11)
I_1, I_2	thrust loading integrals (eqs. 16,17)
J_1, J_2	power loading integrals (eqs. 18,19)
L	lift
n	revolutions per second
P	shaft power (kW)

P_c power coefficient $(P_c \equiv 2P/\rho V^3 \pi R^2)$
Q propeller shaft torque (Nm)
R propeller tip radius (m)
r propeller general radius (m)
S wing plan or fuselage cross section area (m^2)
T thrust (N)
T_c thrust coefficient $(T_c \equiv 2T/\rho V^2 \pi R^2)$
u axial velocity of fuselage flow field at r (m/sec)
$\overline{u}V$ average axial velocity at r (m/sec)
V flight velocity (m/sec)
v radial velocity of fuselage flow field at r (m/sec)
v' displacement velocity (m/sec); see fig. 1
W resultant velocity at blade element $(\vec{W} = \vec{V} + \vec{\Omega r} + \vec{w})$ (m/sec)
w induced velocity at blade element $(\vec{w} = a\vec{V} + a'\vec{\Omega r})$ (m/sec)
w_s slipstream velocity (incremental) (m/sec)
x velocity ratio $(x \equiv \Omega r/V)$
y spanwise location (m)

α section angle of attack (rad); $\alpha°$ (degrees)
β section blade setting angle (rad); $\beta°$ (degrees)
Γ circulation (m^2/sec)
ζ displacement velocity ratio $(\zeta \equiv v'/V)$
η efficiency $(\eta = T_c/P_c \equiv (V/nD)C_T/C_P)$
λ advance ratio $(\lambda \equiv V/\Omega R)$
ξ radius ratio $(\xi \equiv r/R)$
ρ air density (kg/m^3)
σ blade solidity $(\sigma \equiv Bc/2\pi r)$
ϕ helix angle (rad); $\phi = \beta - \alpha$
Ω shaft speed (rad/sec)

TABLE 2

POWERED HANG GLIDER PROPELLERS
V = 13.41 m/sec (30 mph)
7.457 kW (10 hp) @ 8000 engine rpm
ρ = 1.225 kg/m³ (760 mm Hg, 15°C)

Gear Ratio	2R m	P_c	ζ	T_c	η	pitch diameter	$\pi\lambda$
1:1	0.690	13.500	2.544	4.650	0.344	0.356	0.146
9:27	1.000	6.426	1.778	2.888	0.449	0.507	0.288
9:27	1.219	4.323 3.881	1.283 -----	2.179 2.103	0.504 0.541	0.361	0.220
9:37	1.372	3.348 3.145	1.151 -----	1.840 1.821	0.550 0.579	0.450	0.301

FIG. 1 VORTEX SHEET MOTION
MINIMUM INDUCED LOSS PROPELLER

DISPLACEMENT VELOCITY

$$w_{axial} = v'\cos^2\phi_s$$

$$w_{swirl} = v'\cos\phi_s\sin\phi_s$$
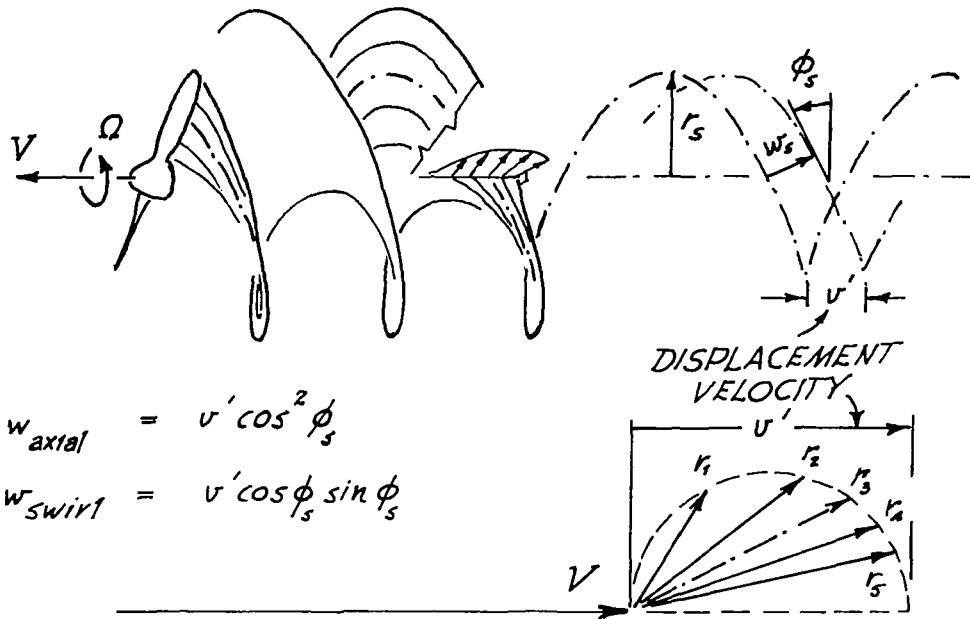
FIG. 2 PRANDTL'S VELOCITY FACTOR, F

$$\frac{2\pi R}{B}\cdot\frac{\lambda}{\sqrt{\lambda^2+1}}$$

$$\lambda = \frac{V}{\Omega R}$$

$$f = \frac{B}{2}\frac{\sqrt{\lambda^2+1}}{\lambda}\left(1-\frac{r}{R}\right)$$

$$Fv'\cos\phi\sin\phi$$

$$Fv'\cos^2\phi$$

$$v'\cos\phi$$

$$f = \pi\left(\frac{x}{s}\right)$$

$$F' = \frac{2}{\pi}\cos^{-1}(e^{-f})$$
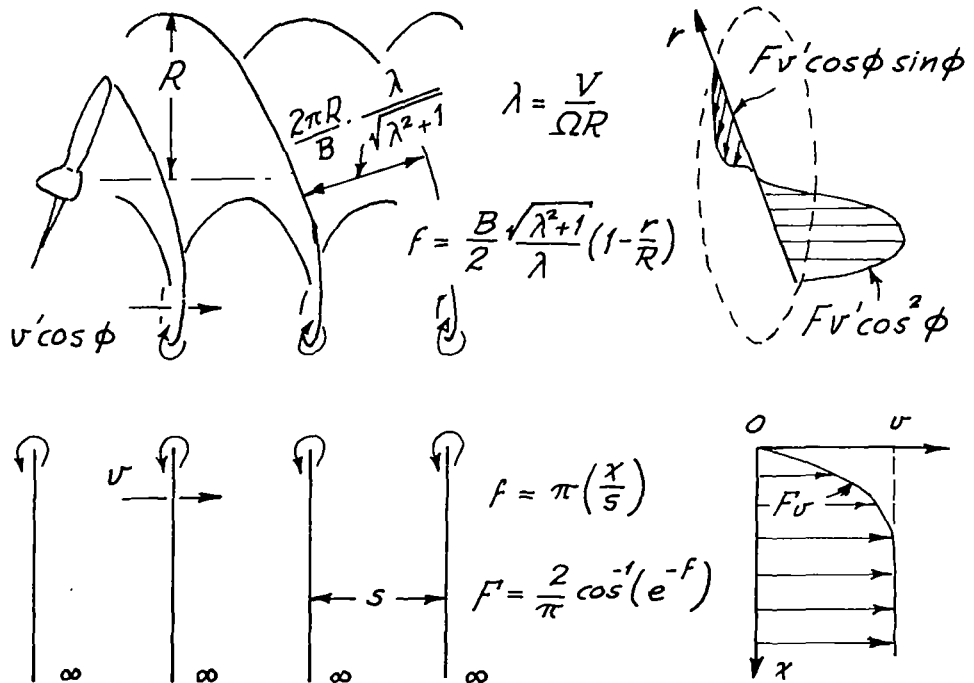
FIG. 3 RADIAL CIRCULATION DISTRIBUTIONS
MINIMUM INDUCED LOSS PROPELLERS

$$B\Gamma = 2\pi r F v' \cos\phi \sin\phi$$

$$\frac{B\Omega\Gamma}{2\pi V v'} = \frac{F' x^2}{x^2 + 1} \; ; \; x \equiv \frac{\Omega r}{V}$$

BETZ u. PRANDTL
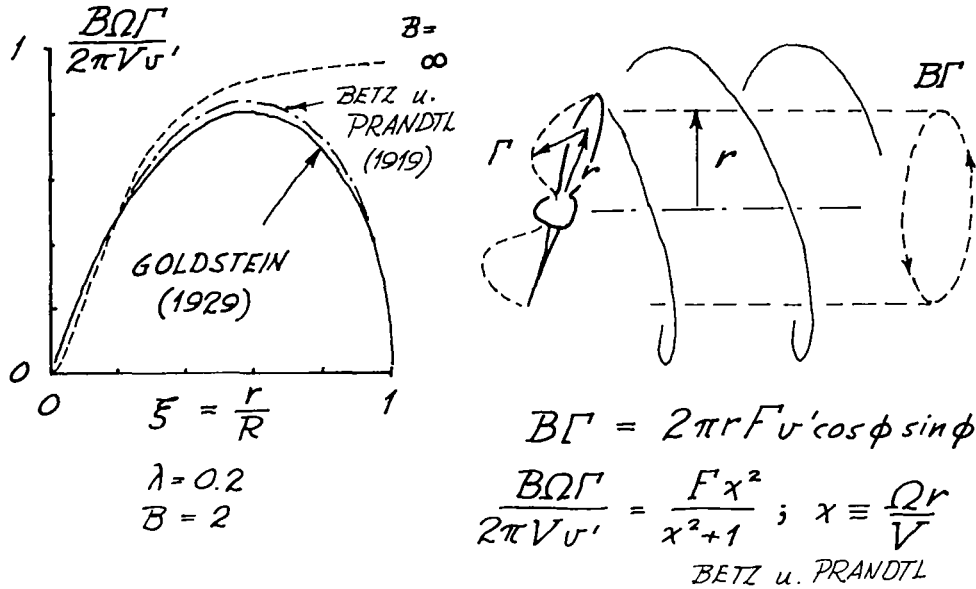
FIG. 4 RADIALLY GRADED MOMENTUM THEORY
INDUCED VELOCITY CALCULATION

$$\frac{dT}{dr} \rightarrow \frac{a}{\bar{u}+a} = \frac{1}{4} \cdot \frac{\sigma C_y}{\sin^2\phi} \cdot \frac{1}{F}$$

$$\frac{1}{r} \cdot \frac{dQ}{dr} \rightarrow \frac{a'}{1-a'} = \frac{1}{4} \cdot \frac{\sigma C_x}{\sin\phi \cos\phi} \cdot \frac{1}{F}$$

$$\bar{u} \equiv \frac{u}{V} \; ; \; \sigma = \frac{Bc}{2\pi r}$$

$$\phi = \beta - \alpha = \tan^{-1}\left[\frac{\bar{u}\lambda}{\xi} \cdot \frac{1+a}{1-a'}\right]$$

$$C_y = F_l \cos\phi - F_d \sin\phi$$

$$C_x = F_l \sin\phi + F_d \cos\phi$$

299
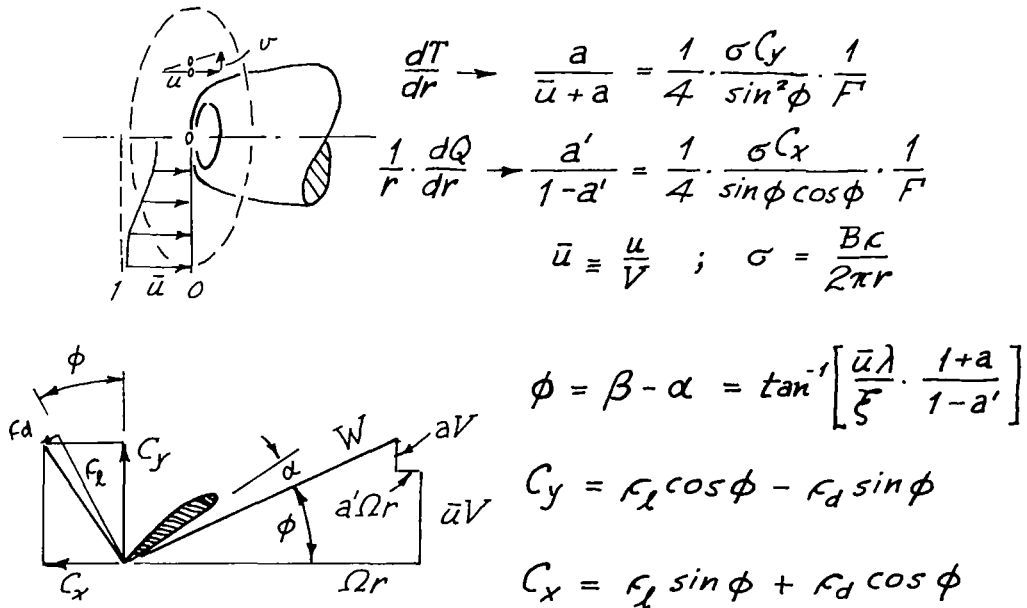
FIG. 5 RADIALLY GRADED MOMENTUM THEORY
$\frac{1}{4}$ SCALE McCAULEY 1C160

CALCULATIONS BY
PETER DUNBECK

C_T

η

C_P

—— ISOLATED

--- GROSS ⎤ WITH
-·- NET ⎦ BODY
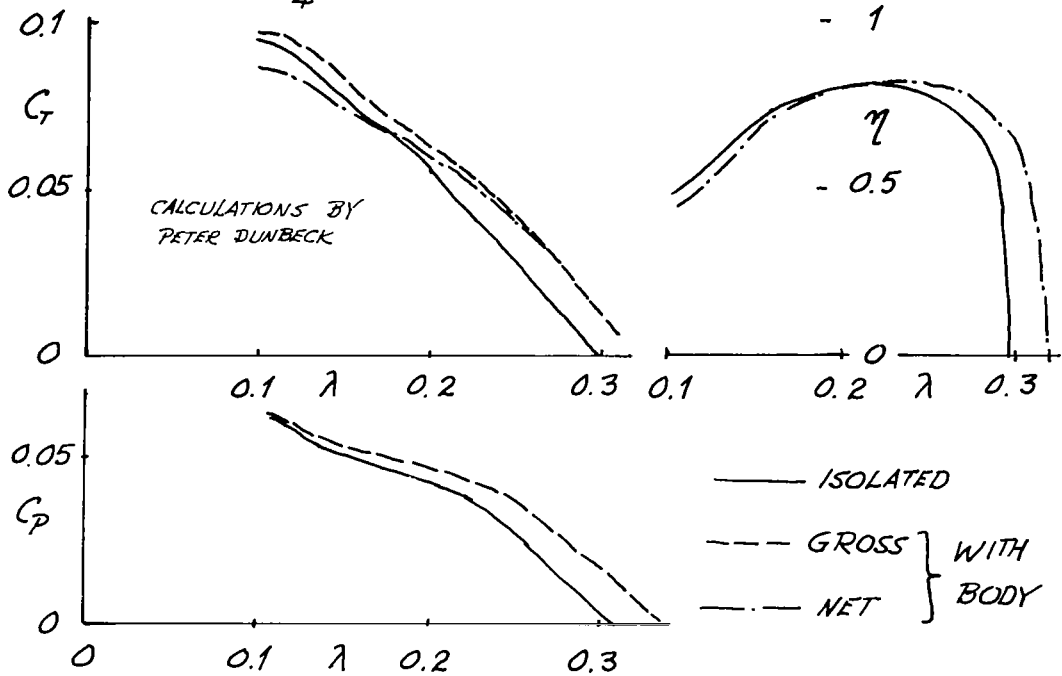
FIG. 6 PROPELLER DESIGN FUNCTIONS
MAN POWERED AIRPLANE

$B = 2, \lambda = 0.2278$

G

$\frac{J_1}{4}$

$\frac{J_2}{2}$

$\frac{i_1}{4}$

$\frac{i_2}{2}$

$\xi \quad 0.5 \quad \frac{r}{R}$

D/L
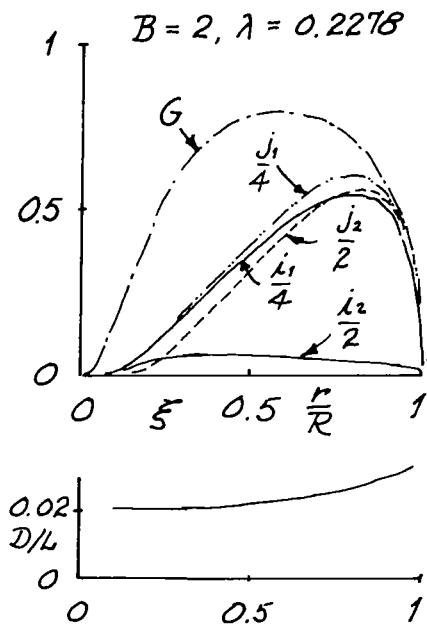
$R = 1.905\,m\ (6.25\,ft)$
$V = 5\,m/sec\ (11.2\,mph)$
$\Omega = 11.52\,rad/sec\ (110\,rpm)$
$T = 53.3\,N\ (11.8\,lbs;\ 1°climb)$
$\rho = 1.178\ kg/m^3$

$i_1 = dI_1/d\xi \quad I_1 = 1.2125$
$i_2 = dI_2/d\xi \quad I_2 = 0.0888$

$j_1 = dJ_1/d\xi \quad J_1 = 1.3151$
$j_2 = dJ_2/d\xi \quad J_2 = 0.5626$

$T_c = 0.3175 \rightarrow \zeta = 0.2671$
$P_c = 0.3914 \leftarrow \eta = 0.8113$

$\pi\lambda\left[1 + \frac{\zeta}{2}\right] = 0.8114$
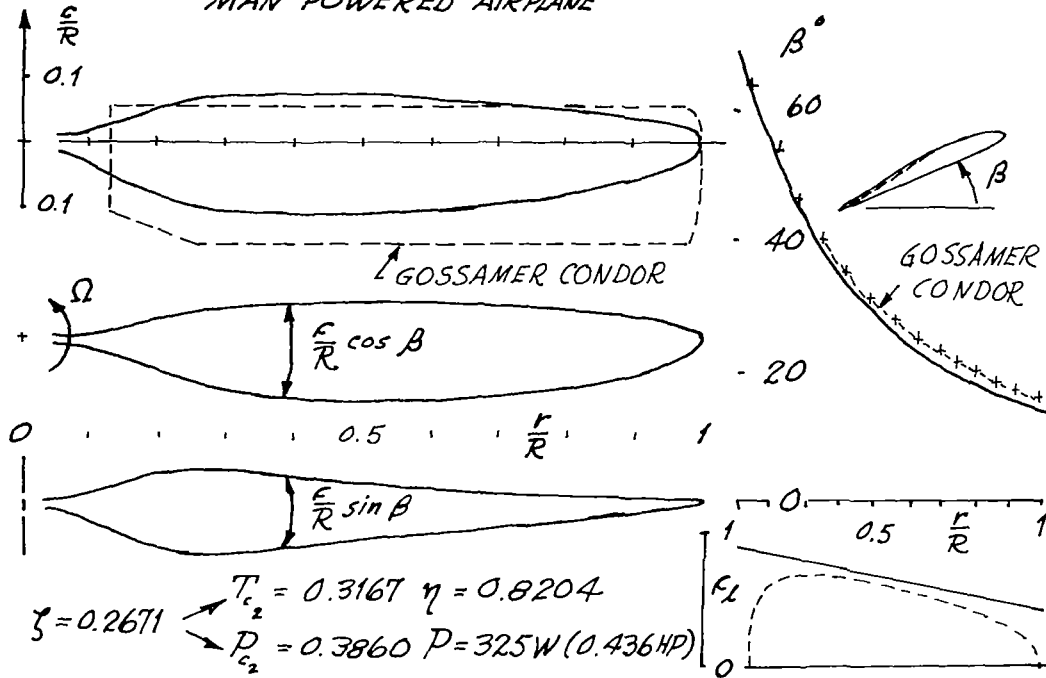
FIG. 7 PROPELLER GEOMETRY
MAN POWERED AIRPLANE

$\frac{c}{R}$

0.1

0.1

GOSSAMER CONDOR

Ω

$\frac{c}{R} \cos \beta$

$\frac{r}{R}$

0.5

$\frac{c}{R} \sin \beta$

$\zeta = 0.2671$

$T_{c_2} = 0.3167$ $\eta = 0.8204$

$P_{c_2} = 0.3860$ $P = 325 W (0.436 HP)$

$\beta°$

60

40

20

GOSSAMER CONDOR

β

$\frac{r}{R}$

0.5

F_L

FIG. 8 POWERED HANG GLIDER PROPELLER OPTIONS

P

8

6

4

HP

4

KW

2

2

12.2 m

(40')

$\left(\frac{L}{D}\right)_{max} = 6.68$

0.5 m/sec
(100 fpm)

level
flight

DIAMETER × PITCH mm	rpm
1372 × 617	1946
1219 × 440	3000
1000 × 507	3000
690 × 240	8000

113 Kg (250 lbs)

10   20   30   mph   40

0   5 V 10 m/sec   15
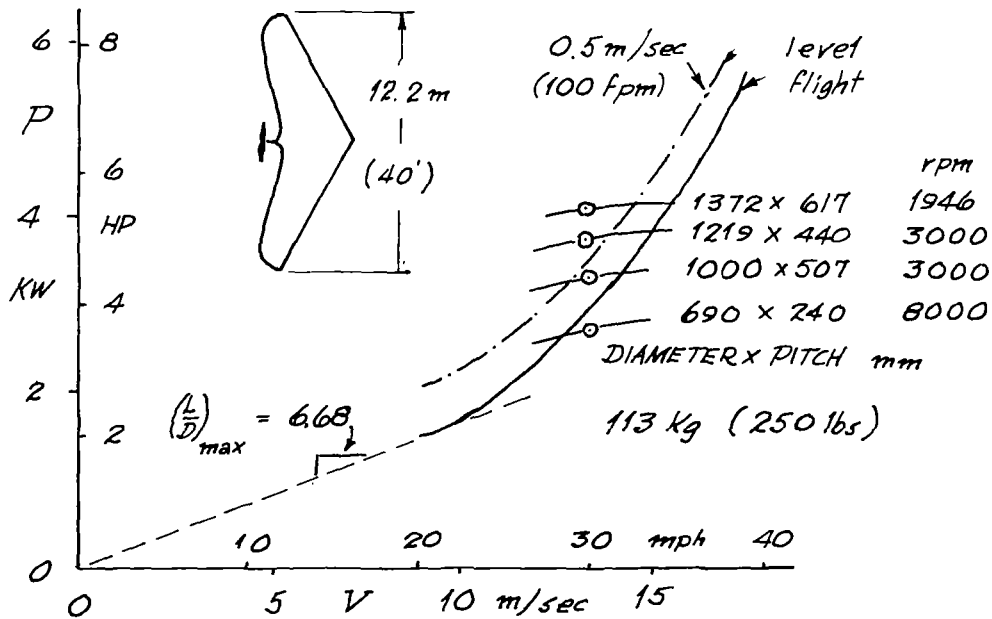
FIG. 9 PROPELLER GEOMETRY
POWERED HANG GLIDER

$\lambda = 0.09596$ $B = 2$

$I_1 = 1.6362$
$I_2 = 0.0329$

$J_1 = 1.8722$
$J_2 = 0.8993$

$\frac{c}{R} \cos \beta$

39.61°   21.93°   14.56°   11.42°   10.00°

58.24°   28.82°   17.55°   12.68°   10.20°

$\frac{c}{R} \sin \beta$

$P_{c_1} = 3.348 \rightarrow \zeta = 1.151$ $\eta_1 = 0.550$

$\zeta = 1.151 \rightarrow P_{c_2} = 3.146$ $\eta_2 = 0.578$
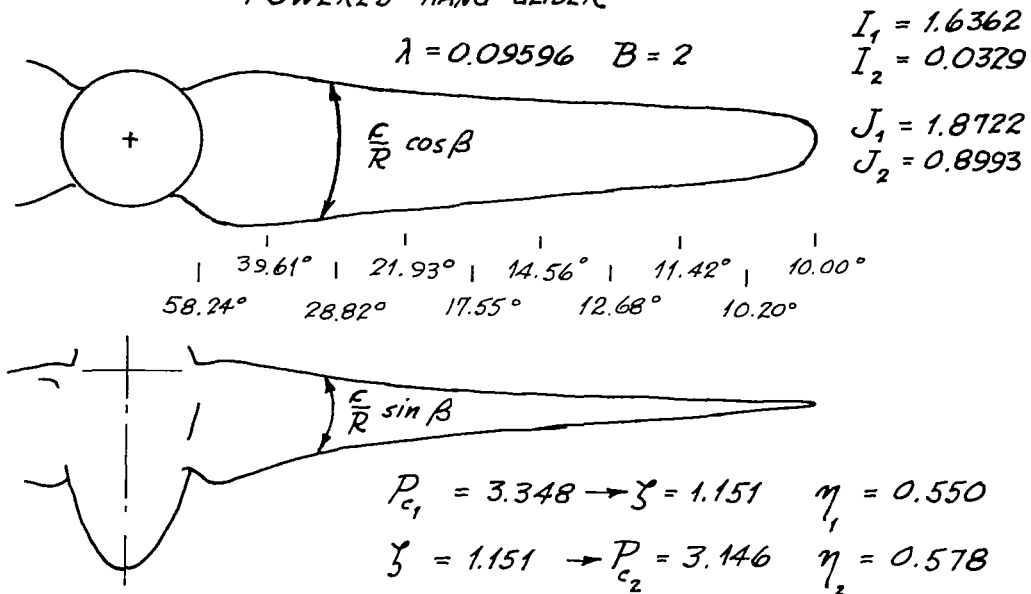
1372 mm DIAMETER x 617 mm PITCH

FIG. 10 POSSIBLE DESIGN POINT PERFORMANCE
RYSON ST-100 MOTORSOARER

sea level

1981 m (6500')

P

100 ——
HP
SHAFT P

80

60 — 80

KW

60

40

1981 m

20

DRAG
UNCERTAIN

40   80   120   160 mph

0   20   40   V   60 $\frac{m}{sec}$ 80

sea level

① CLIMB
74.57 Kw
2750 rpm

② V_{max}
74.57 Kw
2750 rpm
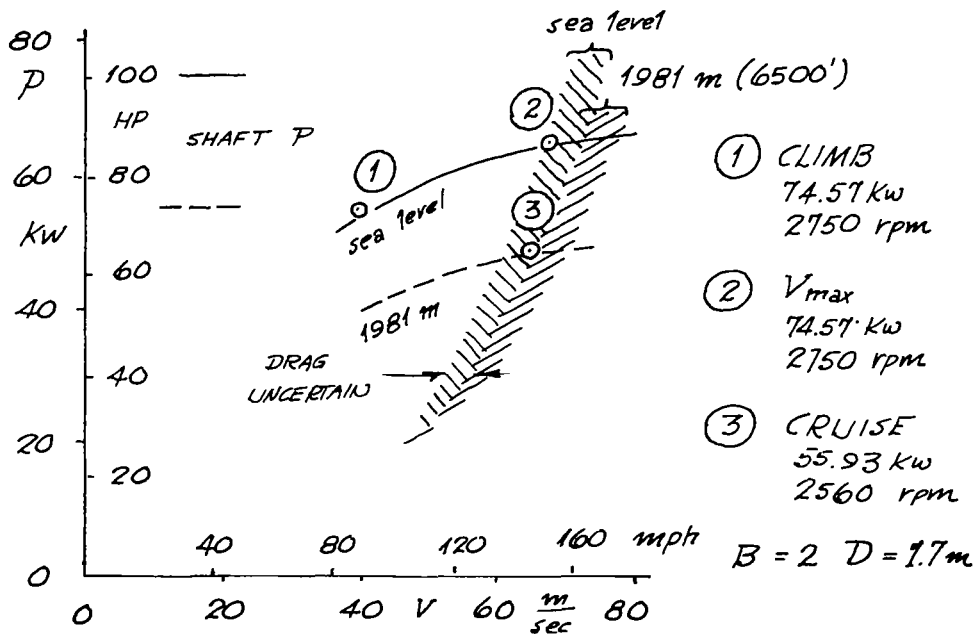
③ CRUISE
55.93 Kw
2560 rpm

$B = 2$ $D = 1.7m$

FIG. 11 COMPROMISE PROPELLER GEOMETRY
RYSON ST-100 MOTORSOARER